Microporous and Mesoporous Materials 178 (2013) 119–122

Contents lists available at SciVerse ScienceDirect

Microporous and Mesoporous Materials

journal homepage: www.elsevier.com/locate/micromeso

Signatures of normal and anomalous diffusion in nanotube systems by NMR

M. Dvoyashkin [a,b], A. Wang [b], A. Katihar [b], J. Zang [c], G.I. Yucelen [d], S. Nair [c], D.S. Sholl [c], C.R. Bowers [a,*], S. Vasenkov [b,*]

[a] Department of Chemistry, University of Florida, Gainesville, FL 32611, USA
[b] Department of Chemical Engineering, University of Florida, Gainesville, FL 32611, USA
[c] School of Chemical & Biomolecular Engineering, Georgia Institute of Technology, Atlanta, GA 30332, USA
[d] School of Materials Science and Engineering, Georgia Institute of Technology, Atlanta, GA 30332, USA

ARTICLE INFO

Article history:
Available online 1 March 2013

Keywords:
Anomalous diffusion
Nanotubes
High field PFG NMR
Hyperpolarized Xe NMR

ABSTRACT

This paper reviews results of our recent studies of diffusion of gaseous sorbates in nanotube systems. ^{13}C pulsed field gradient (PFG) NMR at 17.6 T was used to probe diffusion of tetrafluoromethane in aluminosilicate nanotubes at several sorbate loadings. The results of PFG NMR measurements were compared with the corresponding data obtained by molecular dynamics simulations. The diffusion in this system was found to follow the laws of normal (i.e. Fickian) transport. At the same time, experimental data pointing at single-file diffusion were recorded for xenon gas confined inside dipeptide L-alanyl L-valine (AV) nanotubes. These data were obtained by means of high field ^{129}Xe PFG NMR. The PFG NMR data are compared with recently reported hyperpolarized tracer exchange ^{129}Xe NMR in the same material.

1. Introduction

Diffusion studies of gaseous sorbates in systems of one-dimensional nanochannels are of high fundamental interest and also of high relevance for a number of practical applications. Prominent examples of such applications include molecular separation, nanofluidics and catalysis. Confinement of sorbate transport to one-dimension can lead to anomalous diffusion. A particularly interesting case of anomalous diffusion is single-file diffusion (SFD). SFD can be expected when the nanochannel radius is smaller than the diameter of a sorbate molecule. In this case mutual passages of sorbate molecules inside the channels are excluded. As a result, normal diffusion, according to the Einstein relation, $\langle \Delta x^2(t) \rangle = 2Dt$, no longer takes place. Instead, for sufficiently large displacements in the limit of infinitely long single-file channels, the mean square displacement (MSD) grows proportionally to the square root of the diffusion time [1–4]

$$\langle \Delta x^2(t) \rangle = 2F\sqrt{t} \quad (1)$$

where F is the mobility factor. Despite strong interest in single-file diffusion, there are only a few reports of the direct experimental observation of the time scalling of SFD (Eq. (1)) for molecular sorbates [5–7].

Here we present results of microscopic studies of self-diffusion in nanotube systems in which tetrafluoromethane (CF_4) and xenon (Xe) were used as sorbates. Both types of diffusing species are spherical and have similar diameters between 0.4 and 0.5 nm. The systems of aluminosilicate nanotubes [8,9] and self-assembled L-alanyl-L-valine (AV) nanotubes [10,11] were chosen as sorbents. The maximum value of the external radius of the former nanotubes (~0.8 nm) is larger than the sorbate diameter, while the external radius of the latter nanotubes (~0.25 nm) is significantly smaller than the sorbate diameter. Hence, under our experimental conditions normal and single-file types of transport are expected, respectively, for aluminosilicate nanotubes and AV nanotubes.

Self-diffusion studies were performed by ^{13}C and ^{129}Xe pulsed field gradient (PFG) NMR. These studies have benefited from the possibility to combine the advantages of high (up to 30 T/m) magnetic field gradients and high (17.6 T) magnetic field. Application of strong gradients was needed to record slow transport in nanotubes. Using high field was essential to record sufficiently strong signals from nuclei such as ^{13}C and ^{129}Xe. ^{13}C and ^{129}Xe were chosen for the studies reviewed in this paper because of the expectation that under conditions of strong confinement in nanochannels their T_2 NMR relaxation times would be larger than that of the more traditionally used protons. Under our measurement conditions the T_2 NMR relaxation times of sorbates in nanochannels were estimated to be in the range between 1.5 and 2.7 ms for ^{13}C and around 5 ms or larger for ^{129}Xe.

For AV nanotubes, Xe diffusion data obtained by PFG NMR are compared with recently reported studies of tracer exchange of Xe atoms between AV nanotubes and the surrounding gas phase [12,13]. Tracer exchange experiments with Xe become possible due to hyperpolarization of xenon atoms using spin-exchange

* Corresponding authors.
E-mail addresses: russ@ufl.edu (C.R. Bowers), svasenkov@che.ufl.edu (S. Vasenkov).

1387-1811/$ - see front matter © 2013 Elsevier Inc. All rights reserved.
http://dx.doi.org/10.1016/j.micromeso.2013.02.031

optical pumping, leading to a dramatic (up to 10^4 fold) increase of the detected NMR signal [12,14–16].

2. Experimental

Single-walled aluminosilicate nanotubes were synthesized according to the protocol given in the literature [8,9]. The nanotubes consist of uniform channels having an outer diameter of ~2.8 nm and an inner diameter of up to ~1.6 nm. The size of the nanotube aggregates in the sample used in this work ranges from half a micrometer to a few tens of micrometers, while the average length of individual nanotubes was around 0.4 micrometers.

Self-assembled L-alanyl-L-valine forms hydrophobic dipeptide crystalline channels with an inner diameter of 0.51 nm [10,11]. AV nanotubes were commercially purchased from Bachem and used as received. The average length of the nanotubes was around 50 μm.

The size of the nanotube aggregates in the sample of single-walled aluminosilicate nanotubes and the average length of AV nanotubes used in this work were determined from the micrographs recorded by a JEOL 6400 scanning electron microscope (SEM), which is located at the UF Major Analytical Instrumentation Center. Examples of the recorded micrographs are shown in Fig.1.

PFG NMR diffusion measurements were performed using a 17.6 T Bruker BioSpin NMR spectrometer operating at resonance frequencies of 188.6 MHz and 208.6 MHz for ^{13}C and ^{129}Xe, respectively. Magnetic field gradients up to 30 T/m were generated using diff60 diffusion probe (Bruker BioSpin) and Great60 gradient amplifier (Bruker BioSpin). The standard PFG NMR stimulated echo pulse sequence with eddy current delay (PGSTE LED) was used [17]. This sequence can be schematically presented as $\pi/2$-τ_1-$\pi/2$-τ_2-$\pi/2$-τ_1-$\pi/2$-τ_e-$\pi/2$-echo where the gradient pulses are applied during the time intervals τ_1. The absence of disturbing susceptibility effects was confirmed by verifying that the diffusion data obtained for different values of τ_1 were the same within the experimental uncertainty.

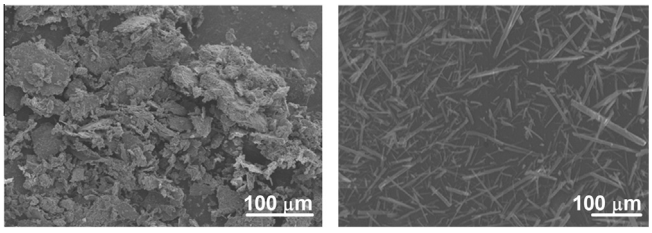

Fig. 1. SEM micrographs of the samples of freeze-dried aluminosilicate single-walled nanotubes (left) and L-alanyl L-valine dipeptide nanotubes (right).

For the case of normal diffusion in randomly oriented channels an expression for a PFG NMR attenuation curve can be presented in the following form [18,19]:

$$\psi_{intra}(q,t_{eff}) = \frac{\sqrt{\pi}}{2}\exp(-q^2 t_{eff} D_\perp) \times erf\left[\left(q^2 t_{eff}(D_{||}-D_\perp)\right)^{1/2}\right] \times \left[q^2 t_{eff}(D_{||}-D_\perp)\right]^{-1/2} \quad (2)$$

where $D_{||}$ and $D_\perp$ are diffusivities parallel and perpendicular to the channel axis, $q = \gamma g \delta$, γ is the gyromagnetic ratio, δ denotes the duration of an applied gradient pulse with amplitude g, and t_{eff} is the effective diffusion time. The value of $D_\perp$ can assume non-zero values due to an occurrence of structural defects making diffusion in the direction perpendicular to the channel axis possible. For the case of SFD in randomly-oriented and defect-free channels similar expression for a PFG NMR attenuation curve can be obtained using Eq. (1) [6,7]

$$\psi_{sf}(q,t_{eff}) = \frac{\sqrt{\pi}}{2} \times erf\left[\left(q^2 F\sqrt{t_{eff}}\right)^{1/2}\right] \times \left[q^2 F\sqrt{t_{eff}}\right]^{-1/2} \quad (3)$$

3. Results and discussion

3.1. Diffusion of tetrafluoromethane in aluminosilicate nanotubes

Carbon-13 PFG NMR attenuation curves for diffusion of ^{13}C-labeled CF_4 in a sample of aluminosilicate nanotubes are presented in Fig. 2(a and b) for the effective diffusion times of 4, 8 and 16 ms. These curves do not have any contributions from CF_4 molecules that diffused only in the gas phase of the sample during the effective diffusion times used. Such contributions were subtracted away from the measured curves. However, the data in Fig. 2 are still expected to have contributions from the long-range diffusion [20], i.e. diffusion under the conditions of fast exchange between the nanotubes interiors and the surrounding gas phase. Hence, the attenuation curves in Fig. 2 were described as a weighted sum of the terms corresponding to the intra-channel and long-range diffusion

$$\psi_{tot}(q,t_{eff}) = p_{lr} exp(-q^2 t_{eff} D_{lr}) + (1-p_{lr})\psi_{intra}(q,t_{eff}) \quad (4)$$

where p_{lr} represents the fraction of molecules performing long-range diffusion with diffusivity D_{lr}, $(1-p_{lr})$ is the fraction of adsorbed molecules never leaving the channels during the effective diffusion time, and ψ_{intra} is given by Eq. (2). Dashed lines in Fig. 2 show the best fit of the attenuation curves using Eq. (4). It is seen in the figure that this equation provides satisfactory description of the measured data. In the presentation of Fig. 2 attenuation curves obtained for different diffusion times are expected to coincide for the case of normal diffusion with time-independent diffusivity(ies) and time-independent fractions of sorbate ensembles diffusing with

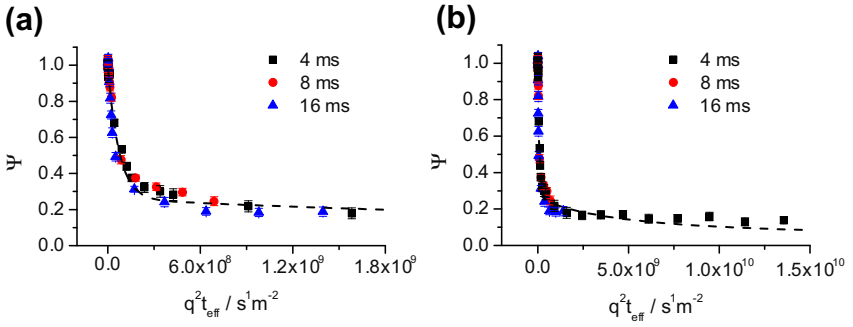

Fig. 2. (a) ^{13}C PFG NMR attenuations curves for CF_4 diffusion in a sample of aluminosilicate nanotubes for effective diffusion times of 4, 8, and 16 ms at 298 K. (b) The same data as in (a) plotted in a larger range of q^2tvalues. The loading of CF_4 inside the nanotubes is 0.51 mol/kg. Dashed lines on both figures show best fit results using Eqs. (2)–(6).

different diffusivities (see Eq. (4)). Good agreement between the attenuation curves corresponding to different effective diffusion times in this figure illustrates that the diffusivities D_{lr}, $D_{||}$ and $D_{\perp}$ as well as p_{lr} can all be considered as time-independent fitting parameters for the range of the diffusion times used. These parameters were found to be time independent for all CF_4 loadings used in this work. The range of the effective diffusion times was limited by the T_1 NMR relaxation time of CF_4 molecules in the channels.

As already discussed above, single-file diffusion is not expected for CF_4 diffusion inside the aluminosilicate nanotubes because the collision diameter of CF_4 (~0.47 nm) is much smaller than the maximum value of the nanotube radius (~0.8 nm). This expectation is confirmed by the observation of the time-independent diffusivity of CF_4 inside the nanotubes ($D_{||}$).

Fig. 3 presents the values of D_{lr} and $D_{||}$ for CF_4 loadings equal to 0.18, 0.32 and 0.51 mol/kg. These diffusivities were obtained from fitting the attenuation curves in Fig. 2 by Eq. (4). The corresponding values of $D_{\perp}$ obtained from the fitting were found to be at least three orders of magnitude smaller than $D_{||}$, indicating that diffusion in the direction perpendicular to the channel axis is negligibly slow. The values of root MSD, which were calculated using the Einstein relation with $D_{||}$ and t_{eff}, were found to be $\leqslant$7 μm. Noting that the average length of individual nanotubes in the sample was several times smaller than this value, $D_{||}$ was assigned to diffusion through several interconnected nanotubes inside nanotube aggregates. Such aggregates can consist of many nanotubes loosely interconnected along the direction of the nanotube lengths.

Fig. 3 also shows for comparison the corresponding results of MD simulations of CF_4 diffusion inside defect-free nanotubes. The simulation details are given in Ref. [21]. It is seen that the values of $D_{||}$ obtained by PFG NMR are approximately one order of magnitude smaller that the corresponding theoretical values. This difference can result from possible transport resistances at the points of connections of individual nanotubes in the nanotube aggregates of the sample used for PFG NMR studies. Such additional transport resistances can slow down the diffusion process along the nanotube directions in the aggregates, which explains why the theoretical diffusivities are larger than the corresponding experimental values.

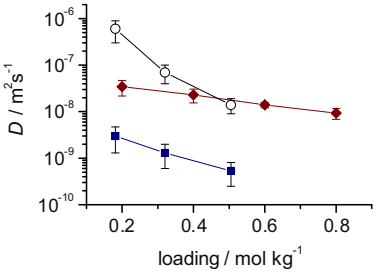

Fig. 3. Dependence of the CF_4 self-diffusion coefficients on CF_4 loading inside aluminosilicate nanotubes at 298 K. Diffusivities were measured by PFG NMR for diffusion inside nanotube aggregates (filled squares) and for diffusion under the conditions of fast exchange between the nanotube aggregates and the surrounding gas phase, i.e. the conditions of long-range diffusion (open circles). Diffusivities were also obtained by MD simulations inside defect-free nanotubes (filled diamonds). The solid lines are shown only as a guide to the eye.

3.2. Diffusion of xenon in AV nanotubes

Xenon-129 PFG NMR attenuation curves were measured for Xe diffusion inside AV nanotubes (line at ~120 ppm) for a broad range of diffusion times between 40 ms and 12 s (Fig. 4). All measurements were performed with the Xe loading of 0.74 mol/kg. Fig. 4a and Fig. 4b present the same PFG NMR diffusion data in two different ways. In Fig. 4a the signal attenuation is plotted as a function of ($q^2 t_{eff}$), as in Fig. 2. According to Eq. (2), attenuation curves measured for different effective diffusion times are expected to collapse onto a single curve when plotted in this way, provided that the diffusion process obeys the Einstein relation with time-independent diffusivity(ies). In the Fig. 4b, the signal attenuation is plotted as a function of ($q^2 t_{eff}^{1/2}$). Eq. (3) requires that in such presentation the attenuation curves for different effective diffusion times collapse into a single curve if the diffusion process obeys the time scaling of SFD (Eq. (1)). The results in Fig. 4 clearly show that the diffusion process of Xe in AV nanotubes obeys the time scaling of SFD. Single-file transport is expected in the considered system because the external radius of the nanotubes (~0.25 nm) is significantly smaller than the diameter of Xe atoms (~0.44 nm).

In contrast to diffusion of CF_4 in the aluminosilicate nanotubes, our PFG NMR data for Xe in samples of AV nanotubes provide no evidence for the existence of the long-range diffusion of Xe under our measurement conditions. The observed absence of the long-range diffusion is in agreement with the observation that even for the largest diffusion time used the root MSDs of Xe atoms inside nanotube channels were at least one order of magnitude smaller than the average length of the nanotubes (around 50 μm). The values of the root MSD of Xe atoms were obtained from the measured attenuation curves using Eqs. (1) and (3). Detailed studies of the dependence of MSD of Xe in AV nanotubes on diffusion time are currently in progress.

As discussed in Ref. [22], the PFG NMR observation of the time scaling of SFD (Eq. (1)) could be caused by normal diffusion in nanochannels that bend and form coils. This and other possible alternative explanations of the observed time scaling of SFD are ruled out by previously published hyperpolarized tracer exchange data in AV nanotubes [12]. In the tracer exchange experiments concentration increase of the labeled by hyperpolarization xenon atoms inside the channels is observed as a function of time (τ) under the conditions when the concentration of all (labeled plus unlabeled) Xe atoms in the channels remain the same at all times.

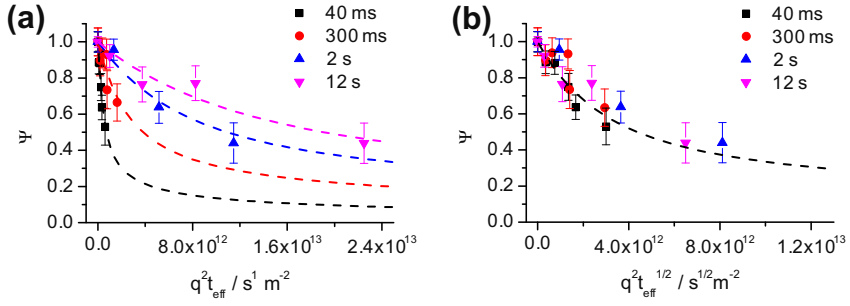

Fig. 4. ^{129}Xe PFG NMR attenuations curves for xenon diffusion inside AV nanotubes for effective diffusion times of 40 ms, 0.3 s, 2 s and 12 s at 298 K. The signal attenuation ψ is plotted as a function of $q^2 t_{eff}$ (a) and also as a function of $q^2 t_{eff}^{1/2}$ (b). The Xe loading inside the nanotubes corresponds to sorption equilibrium with Xe in the gas phase at a pressure of 3 bar. Dashed lines show the results of the best fit using Eq. (3).

Fig. 2a and b of Ref. [12] shows the measured NMR tracer exchange function (points) along with the theoretical predictions for SFD (solid line) and for normal diffusion (ND) (dashed line). The results support the conclusions that the experimentally observed behavior in the PFG NMR data is in agreement with SFD. Bending or coiling of channels is not expected to affect the time dependence of the number of labeled Xe atoms that diffuse into the channels in the hyperpolarized NMR tracer exchange experiment. Moreover, the SEM images of the polycrystalline AV crystals show no evidence of curved, bent, or coiled channels.

4. Conclusions

This paper is a mini-review that focuses on our recent microscopic studies of transport in nanotube systems. ^{13}C PFG NMR was applied to investigate diffusion of tetrafluoromethane in aluminosilicate nanotubes where normal (i.e. Fickian) diffusion was observed. This experimental observation was found to be in agreement with the corresponding results obtained by MD simulations. The experimental diffusivities of CF_4 inside aggregates of aluminosilicate nanotubes were about one order of magnitude smaller than the corresponding theoretical diffusivities inside defect-free nanotubes. This difference was explained by the existence of additional transport resistance at the points of the interconnections between individual nanotubes in aggregates present in the experimentally studied nanotube sample.

On the other hand, ^{129}Xe PFG NMR was used to study Xe transport inside AV nanotubes. The experimental data were found to obey the time scaling of single-file diffusion (Eq. (1)). This observation is consistent with the expectation that Xe atoms are too large to pass one another in the channels of AV nanotubes. Alternative explanations for the observed diffusion time-scaling are ruled out by previously published hyperpolarized tracer exchange studies in AV.

Acknowledgments

PFG NMR data were obtained at the Advanced Magnetic Resonance Imaging and Spectroscopy (AMRIS) facility in the McKnight Brain Institute of the University of Florida. This material is based upon work supported by the National Science Foundation under Grant No. CHE-0957641. SN and DSS acknowledge partial support of this work from the NSF (Awards No. CBET-0846586 and No. CBET-0966582). Any opinions, findings, and conclusions or recommendations expressed in this material are those of the author(s) and do not necessarily reflect the views of the National Science Foundation. Helpful discussions with Prof. H. W. Beckham (Georgia Institute of Technology) are gratefully acknowledged.

References

[1] P.A. Fedders, Phys. Rev. B 17 (1978) 40–46.
[2] J. Karger, Phys. Rev. A 45 (1992) 4173–4174.
[3] M. Kollmann, Phys. Rev. Lett. 90 (2003) 180602.
[4] D.G. Levitt, Phys. Rev. A 8 (1973) 3050–3054.
[5] A. Das, S. Jayanthi, H.S.M.V. Deepak, K.V. Ramanathan, A. Kumar, C. Dasgupta, A.K. Sood, ACS Nano 4 (2010) 1687–1695.
[6] K. Hahn, J. Karger, V. Kukla, Phys. Rev. Lett. 76 (1996) 2762–2765.
[7] V. Kukla, J. Kornatowski, D. Demuth, I. Gimus, H. Pfeifer, L.V.C. Rees, S. Schunk, K.K. Unger, J. Karger, Science 272 (1996) 702–704.
[8] D.Y. Kang, J. Zang, C.W. Jones, S. Nair, J. Phys. Chem. C 115 (2011) 7676–7685.
[9] S. Mukherjee, V.A. Bartlow, S. Nair, Chem. Mater. 17 (2005) 4900–4909.
[10] C.H. Gorbitz, Chem. Eur. J. 7 (2001) 5153–5159.
[11] D.V. Soldatov, I.L. Moudrakovski, E.V. Grachev, J.A. Ripmeester, J. Am. Chem. Soc. 128 (2006) 6737–6744.
[12] C.R. Bowers, C.Y. Cheng, T.C. Stamatatos, G. Christou, AIP Conf. Proc. 1330 (2011) 43–46.
[13] C.Y. Cheng, C.R. Bowers, Chem. Phys. Chem. 8 (2007) 2077–2081.
[14] C.Y. Cheng, C.R. Bowers, J. Am. Chem. Soc. 129 (2007) 13997–14002.
[15] C.Y. Cheng, J. Pfeilsticker, C.R. Bowers, J. Am. Chem. Soc. 130 (2008) 2390–2391.
[16] T. Meersmann, J.W. Logan, R. Simonutti, S. Caldarelli, A. Comotti, P. Sozzani, L.G. Kaiser, A. Pines, J. Phys. Chem. A 104 (2000) 11665–11670.
[17] S.J. Gibbs, C.S. Johnson, J. Magn. Reson. 93 (1991) 395–402.
[18] P. Callaghan, Principles of Nuclear Magnetic Resonance Microscopy, First ed., Oxford University Press, USA, 1994.
[19] S. Naumov, R. Valiullin, J. Karger, R. Pitchumani, M.O. Coppens, Microporous Mesoporous Mater. 110 (2008) 37–40.
[20] J. Kaerger, D.M. Ruthven, Diffusion in Zeolites and Other Microporous Solids, Wiley, New York, 1992.
[21] M. Dvoyashkin, J. Zang, G.I. Yucelen, A. Katihar, S. Nair, D.S. Sholl, C.R. Bowers, S. Vasenkov, J. Phys. Chem. C 116 (2012) 21350–21355.
[22] R. Valiullin, J. Karger, ACS Nano 4 (2010) 3537.